



I. V. Andrianov · J. Awrejcewicz  · A. A. Diskovsky

# Structural design of patient-specific vascular ring stents

Received: 29 June 2022 / Accepted: 6 December 2022 / Published online: 26 December 2022  
© The Author(s) 2022

**Abstract** The expediency of replacing the corrugated ring of a vascular stent with a constant corrugation pitch by a corrugated ring of variable pitch is being investigated. To describe the change in pitch of corrugation, a special function is introduced. The equilibrium and deformation equations were analyzed using the asymptotic homogenization method. The dependence of the radial stiffness of a corrugated ring with a variable pitch of corrugation on the constructive parameters is obtained. The effectiveness of the design under consideration is evaluated by the area of the lumen provided by the vascular stent. Compared to stents with regularly corrugated rings, this area is larger which improves the ring stent efficiency.

**Keywords** Patient-specific vascular stent · Corrugated ring · Asymptotic homogenization method · Structural design

## 1 Introduction

Vascular, intervascular and cardiovascular stents are widely used to restore patency in atherosclerotic coronary arteries and they play an important role in recovering patients from various cardiovascular diseases. It is expected in the coming future that the key issues with regard to high stress, damage and restenosis rate after stent implantation will be reasonably well solved. In addition, it is expected that vascular stents will be both patient-specific and customized for patients.

It is obvious that during mathematical modeling and practical design of vascular stents, there is a need to consider interaction effects between the stent and the artery as well as the influence of the vascular injury on the degree of restenosis [1–7]. In order to achieve optimum stent design, majority of the preliminary investigation relies on employment of the finite element method (FEM).

Rogers et al. [8] used FEM to analyze balloon-artery interactions during stent placement based on the 2D model and linear elastic material properties. Auricchio et al. [9] developed a 3D model to improve stent design, and then Holzapfel et al. [10] estimated the stress introduced within the vessel for a balloon angioplasty and

---

I. V. Andrianov  
Chair and Institute of General Mechanics, RWTH Aachen University, Eilfschornsteinstraße 18, 52062 Aachen, Germany  
e-mail: igor.andrianov@gmail.com

J. Awrejcewicz (✉)  
Department of Automation, Biomechanics and Mechatronics, Lodz University of Technology, 1/15 Stefanowski St., 90924 Lodz, Poland  
e-mail: jan.awrejcewicz@p.lodz.pl

A. A. Diskovsky  
Department of Information Technology, Dnipropetrovsk State University of Internal Affairs, Gagarina Ave 26, Dnipro 49005, Ukraine  
e-mail: alex\_diskovskiy@ukr.net

employed the Palmaz-Schatz procedure with a help of FEM. The study of Lally et al. [11] based on FEM was focused on testing the hypothesis that two different stent designs imply different levels of stress in an atherosclerotic artery. The authors claim that their results correlated with observed clinical restenosis rates.

Timmins et al. [12] examined the effects of varying stent designs and atherosclerotic plaque stiffness on the arterial wall biomechanic features. Various 3D FEM models were developed for calculation of displacement, pressure and contact boundary conditions. A non-uniform mesh was employed, whereas displacements were interpolated using quadratic Lagrange functions and contacting bodies were modeled by a continuous non-uniform rational B-splines surface. It was concluded that stent design differences can impose dramatically different stress fields.

Timmins et al. [13] used a combination of computational modeling and in vivo analysis to study the pathobiologic response to two stent designs that impose greater or lesser levels of stress on the artery wall.

Schmidt et al. [14] studied the 3D self-expanding stent with regard to technical parameters obtained in the clinical tests. Kokot et al. [15] employed FEM to analyze the crimping process of the polymer stent. Their results can be used for designing the bioresorbable self-expanding vascular stents. Qiu et al. [16] used FEM to study mechanical properties of bioresorbable polymeric stents. Wei et al. [17] reported a new design method to improve biodegradable polymeric stent mechanical properties. It was based on the force analysis of supporting rings and bridges during stent implantation. Radial force and axial foreshortening of the open C-shaped stent were studied using FEM. The numerical results were validated by the carried out laboratory experiments including stent expansion and planar compression.

Liu et al. [18] investigated local hemodynamic environment changes caused by straightening phenomenon and the relationship between straightening and in-stent restenosis by using the different 3D FEM models (ANSYS). It was shown that the straightening process altered the wall shear stress and flow patterns distribution and decreased the wall shear stress. Bernini et al. [19] developed a computational model exhibiting effects of stent sizing. They predicted the optimal oversizing ratio for self-expanding Nitinol stents being similar to the clinical observations.

Currently, the creation of a patient-specific vascular stent is becoming a priority. At the same time, special attention is paid to the development of a stent that takes into account the shape of the blood vessel of a particular patient. Such a stent is capable of taking on a shape identical to that of a blood vessel after deployment and deformation. Auricchio et al. [20] studied such vascular stents, having a small degree of curvature. Morlacchi et al. [21] analyzed the case when two stents were used for the affected part of the curved blood vessel, which overlapped that considered in the curved part. Ragkousis et al. [22] evaluated the longitudinal deformation of models of three stent designs. Han and Lu [23] developed a non-uniform Poisson ratio vascular stent for patients with a linearly curved vessel. In addition, the optimization of stent structures was considered, while the studied blood vessels had a small curvature. In [24], the authors reviewed the various structural design of vascular stents. The fabricating methods to achieve optimized vascular stents were illustrated and discussed.

In the work on designing a patient-specific vascular stent, insufficient attention was paid to the fact that the plaques encountered in the vessel wall (Fig. 1) also have specific sizes and shapes. He et al. [25] developed personalized nitinol stent designs for lesion-specific arteries with one and two opposite focal plaques. Both lumen gain and shape of the stent were significantly improved in comparison with the commercial stents.

Majority of the discussed works are devoted to modeling and analysis of the vascular stents based on the FEM.

It should be emphasized that the distribution of the thickness of vascular plaques is not constant in the circumferential and longitudinal directions. This leads to the fact that radial pressure of variable intensity acts on the stent from the side of the vessel wall after installation. Currently, this factor is not taken into account, and stents are designed with excessive radial stiffness, determined by the maximum value of the radial pressure. Excessive radial stiffness leads to oversized cross sections of the fibers of the stent, which adversely affects its medical performance. The resolution of this contradiction can be the design of stents with variable stiffness in the circumferential direction. For this, it is proposed to use a stent consisting of corrugated rings with a variable corrugation pitch. Such corrugation was considered earlier in [26–31] for shell structures and showed higher efficiency for loads of variable intensity. It can be expected that a variable pitch stent that is properly oriented with respect to the plaques will deform less radially than a regularly shirred stent, and thus provide a greater opening for blood flow.

It should be noticed that vascular plaques change their geometric characteristics not only along the circumference, but also along the vascular directions. Therefore, another possibility of development of the proposed approach stands for design of each individual link of the stent—a corrugated ring, depending on its location along the vascular direction.”

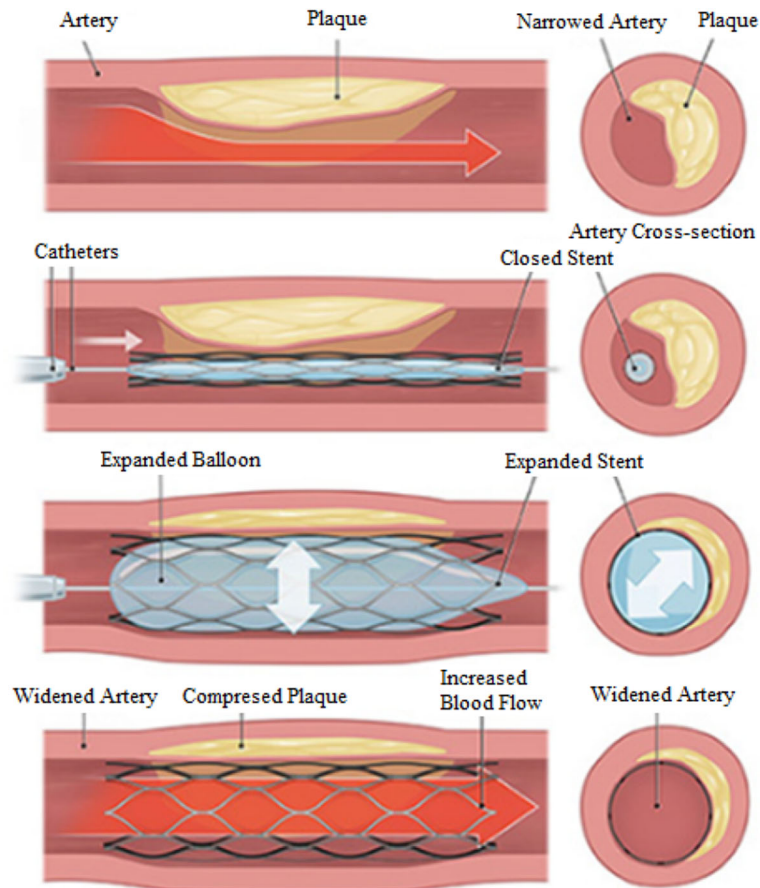


**Fig. 1** An example of a vascular plaque and ballooning scheme [NQ Vascular Townsville review 2022, Open Access]

The paper is organized in the following way. Section 2 deals with simulation of the external load acting on the stent after ballooning, while Sect. 3 presents the stent model. Geometric characteristics of the stent are discussed in Sect. 4, and Sect. 5 reports the equilibrium equations. The latter are homogenized in Sect. 6. Section 7 presents the displacement and strain equations, and Sect. 8 is aimed on evaluation of the effectiveness of the use of variable pitch corrugations. The obtained results are briefly summarized in Sect. 9.

## 2 Simulation of the external load acting on the stent after ballooning

Geometrically, vascular plaques can be divided into two types: with complete (Fig. 2) and partial (Fig. 1) coverage of the vessel around the circumference. The paper considers vascular plaques of the first type, the boundary of which is modeled in the polar coordinate system on the interval  $[0, 2\pi]$  by the power function. At the same time, the conjugation conditions for the function (2) and the first two derivatives (3), (4) must be satisfied at the boundaries of the interval. It is natural to represent this function as a fourth-degree polynomial of the following form

$$\rho(\varphi) = R - (a\varphi^4 + b\varphi^3 + c\varphi^2 + e\varphi + d). \quad (1)$$

and the following boundary conditions

$$\rho(0) = \rho(2\pi); \quad (2)$$

$$\rho_\varphi(0) = \rho_\varphi(2\pi), \quad (3)$$

$$\rho_{\varphi\varphi}(0) = \rho_{\varphi\varphi}(2\pi), \quad (4)$$

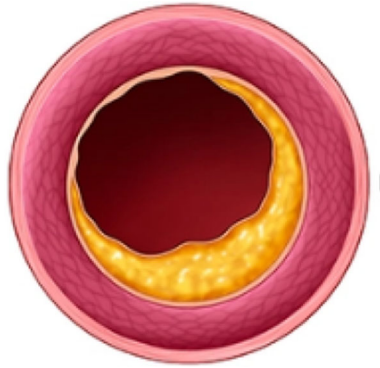


**Fig. 2** An example of a vascular plaque with full circumferential coverage of the vessel [Last reviewed by a Cleveland Clinic medical professional on 02/25/2022]

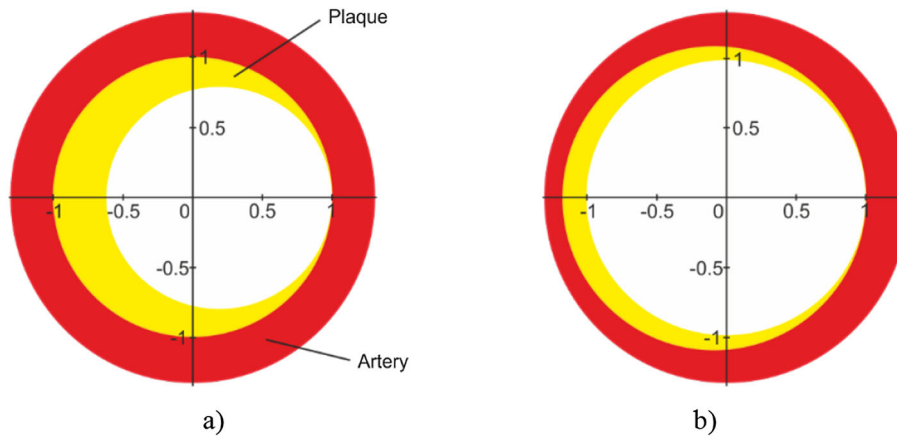


**Fig. 3** Example of a vascular plaque model (5) before (a) and after (b) ballooning when the balloon restores the natural shape of the vessel  $R = 1$ , and the plug is pressed into the vessel wall

where  $(\cdot)_{\varphi} = \frac{d}{d\varphi}$ .

Substituting expression (1) into conditions (2)–(4), we obtain

$$\rho = R - a \left( \varphi^4 - 4\pi\varphi^3 + 4\pi^2\varphi^2 + \frac{d}{a} \right), \quad (5)$$

where the values of the parameters  $a$ ,  $d$  must not violate the following inequality

$$0 \leq \rho \leq R. \quad (6)$$

The proposed mathematical model of vascular plaque (5) is only demonstrative in terms of assessing the possibility of using vascular stents with corrugated ring having a variable pitch of corrugation. In other words, real vascular plaques require more complex mathematical modeling. A review of more adequate models of plaques is given in Ref. [25] where modeling of one and two opposite focal plaques, based on medical imaging of patients and computer simulations, is demonstrated. The so-called silico analysis is aimed on assessment of stent performance in the diseased arteries, and hence, any constructive proposal to improve a stent design and fabrication plays a crucial role for solving many health problems of patients. It is well known and recognized that personalized designs significantly increase the lumen gain, reduce the stresses in the media layer, and improve the lumen shape compared to the commercial nitinol stent. The approaches to modeling vascular plaques described in [25] can be used to develop and refine the method proposed in this paper for structural design of patient-specific vascular ring stents.

Figure 3 shows an example of a vascular plaque model (5) with the following fixed parameters:  $R = 1$ ;  $a = 0.003$ ;  $d = 0.01$ , before (a) and after (b) ballooning.



**Fig. 4** Vascular ring stent. Wikimedia Commons, the free encyclopedia, 2022 [Online; accessed May 2022]

As a result, during ballooning, plaque is pressed into the wall of the artery and the inner side of the artery takes the shape of a circle (Fig. 3b). This shape is further supported by a stent, which is acted upon by a distributed external pressure from the side of the artery wall  $q$ . The intensity of such pressure will not be uniform due to the uneven thickness of the plaque. Determining the pressure intensity distribution  $q$  is a non-trivial task and is specified with the elastic properties of the artery wall and plaque. In order to assess the feasibility of using corrugated rings with a variable corrugation pitch for a stent, we restrict ourselves to a simplified scheme of vessel wall deformation after balloting and we assume that the pressure intensity will be proportional to the plaque thickness distribution. At the same time, the refinement of the pressure distribution law does not change the proposed research scheme. Thus, the wall of the artery is considered as an elastic Winkler-Fuss foundation with some linear characteristics, and hence,

$$q = k \left( R + a \left( \varphi^4 - 4\pi\varphi^3 + 4\pi^2\varphi^2 + \frac{d}{a} \right) \right), \quad (7)$$

where  $k$  stands for the proportionality factor.

Another characteristic feature of vascular plaque is the position of maximum and minimum of its thickness, which for the vascular plaque model (5) obeys the following restrictions

$$\max q = q(\pi), \quad \min q = q(0). \quad (8)$$

It should be noted that the scheme proposed by us makes it possible to calculate vascular plaques that do not completely cover the artery along the circumference (Fig. 1).

### 3 Unit cell of stent model

Usually, the unit cell of vascular stent (Fig. 4) is a regularly corrugated ring (Fig. 5).

The vector equation of the axial line of a regularly corrugated ring (Fig. 5) in a cylindrical coordinate system takes the form

$$\bar{r} = R\bar{e}_1 + Z(n\varphi)\bar{e}_3, \quad (9)$$

where  $Z = H\theta(n\varphi)$ ;  $\theta(n\varphi)$ ,  $\theta_\varphi(n\varphi)$ ,  $\theta_{\varphi\varphi}(n\varphi)$  are the continuous periodic functions with period  $2\pi/n$ ;  $n$  is the number of corrugation waves.

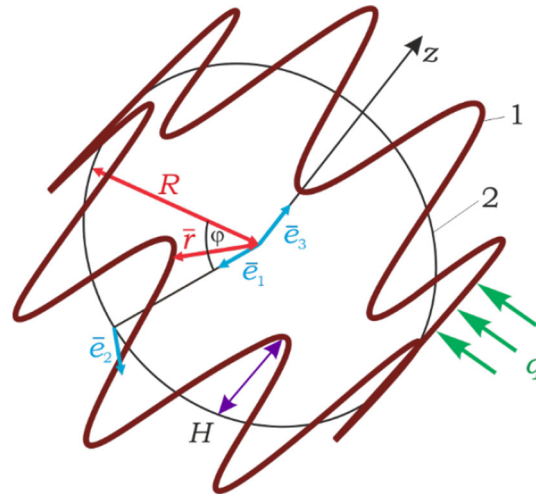


**Fig. 5** Corrugated ring as the unit cell of stent 1 (2 is a circle equidistant from the tops of the corrugation;  $H$  is the amplitude of the corrugation;  $q$  stands for the distributed load normal to the cylindrical surface of radius  $R$ , acting from the side of the vessel walls)

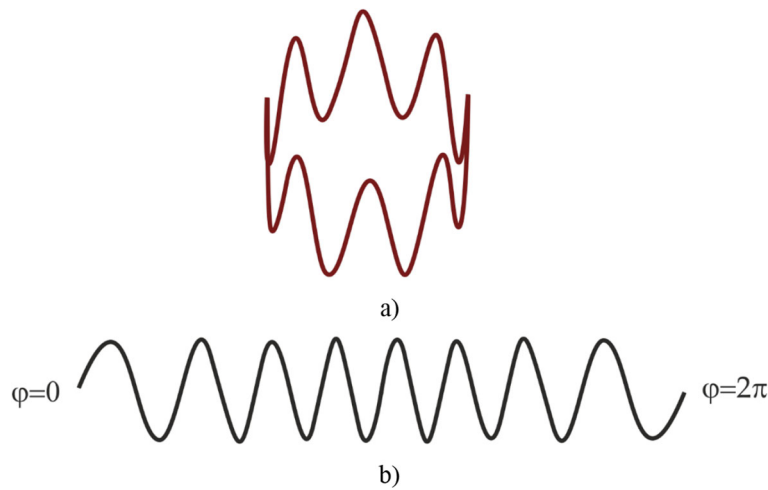


**Fig. 6** Example of a ring with a variable pitch of the corrugation (a) and its development (b);  $z = \sin(nf(\varphi))$ ;  $n = 8$ ;  $\alpha = 0.0008$ ;  $f = \alpha(\varphi^5 - 5\pi\varphi^4 + \frac{20}{3}\pi\varphi^3 + 20\pi^2(\pi - 1)\varphi^2 + (\frac{40}{3}\pi^3 - 16\pi^4 + \frac{1}{\alpha})\varphi)$ .

The smooth function  $\theta(n\varphi)$ , which determines the shape of the corrugation, is symmetric with respect to the circle (curve 2 in Fig. 5),  $-1 \leq \theta(n\varphi) \leq 1$ ,  $0 \leq \varphi \leq 2\pi$ .

For a ring with a variable corrugation pitch, an example of which is shown in Fig. 5, the vector equation can be written as

$$\bar{r} = R(\bar{e}_1 + z(nf(\varphi))\bar{e}_3), \tag{10}$$

where  $f(\varphi)$  stands for a function, the derivative of which determines the change of the corrugation pitch, and  $z = Z/R$  (Fig. 6).

The choice of the function  $f(\varphi)$  will be carried out with the condition that the number of corrugation waves (11) is preserved. This condition is important for mating the stent rings, each of which can obey different laws of change in the corrugation pitch. We have

$$f(0) = 0; f(2\pi) = 2\pi; f(\varphi) > 0, f_\varphi(\varphi) > 0 \text{ for } \varphi \in [0, 2\pi]. \tag{11}$$

The conditions (11) are supplemented by the continuity conditions as follows

$$f_\varphi(0) = f_\varphi(2\pi); f_{\varphi\varphi}(0) = f_{\varphi\varphi}(2\pi); f_{\varphi\varphi\varphi}(0) = f_{\varphi\varphi\varphi}(2\pi). \tag{12}$$

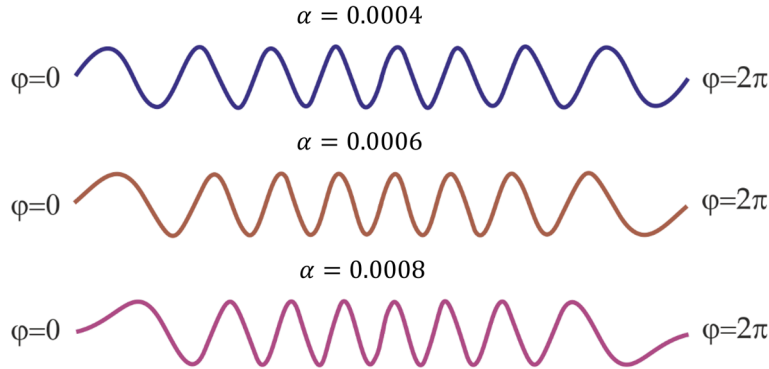


**Fig. 7** Influence of the value of the coefficient  $\alpha$  (14) on the corrugation pitch change for the function (13), where  $z = \sin(nf(\varphi))$ ;  $n = 8$

As an example, we define  $f(\varphi)$  as a power function on the interval  $[0, 2\pi]$  and periodically continue it with a period  $2\pi$ . We have

$$f = \alpha \left( \varphi^5 - 5\pi\varphi^4 + \frac{20}{3}\pi^2\varphi^3 - \left( \frac{8}{3}\pi^4 - \frac{1}{\alpha} \right) \varphi \right), \tag{13}$$

where  $a$  is the coefficient that determines the rate of change of the corrugation step. It follows from constraints (11) that

$$0 < \alpha < 0.00087. \tag{14}$$

Written an approximate formula for the increment of the step function and equating this increment to the period of the function  $Z(n\varphi)$ , the following estimation holds

$$\Delta f \approx f_{\varphi}(\varphi)\Delta\varphi = \frac{2\pi}{n}, \tag{15}$$

and the law of change of the corrugation pitch is governed by the following simple formula

$$\Delta\varphi = \frac{2\pi}{nf_{\varphi}(\varphi)}. \tag{16}$$

For function (13), the decrease ( $f_{\varphi}(\varphi) > 1$ ) will be in the interval  $[0.44\pi, 1.56\pi]$ , and increase in the corrugation pitch ( $f_{\varphi}(\varphi) < 1$ ) in the rest of the areas. This property can be used to achieve a proper orientation of the stent relative to the plaque.

Figure 7 shows the influence of the value of the coefficient  $\alpha$  (14) versus the change in the corrugation pitch.

Since stent radial stiffness will depend on the nature of the corrugation, therefore, by choosing the function (13), it is possible to control the change of the stiffness along circumference direction, increasing it where the plaque is thicker.

#### 4 Geometric characteristics

The required geometric characteristics of the axial line of the corrugated ring with variable corrugation pitch (10), i.e., differential  $ds$ , curvature  $k$  and torsion  $\chi$  can be found using well-known differential geometry formulas [32]:

$$ds = RAd\varphi, \tag{17}$$

$$k = \frac{B}{RA^3}, \tag{18}$$

$$\chi = -\frac{\beta + \beta_{\varphi}\varphi}{RB^2}, \tag{19}$$

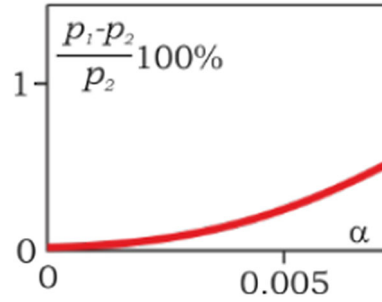


**Fig. 8** Influence of the value of the coefficient  $\alpha$  on the perimeter  $p_1$  of the corrugated ring of variable pitch (13);  $p_2$  is the perimeter of a regularly corrugated ring (9)

where  $(\cdot)_\varphi = \frac{d}{d\varphi}$ ,  $A = \sqrt{1 + \beta^2}$ ,  $\beta = z_\varphi$ ,  $B = \sqrt{1 + \beta^2 + \beta_\varphi^2}$ .

Principal normal unit vectors  $\bar{e}'_1$ , tangent  $\bar{e}'_2$  and binormals  $\bar{e}'_3$  of the centerline are (Fig. 6)

$$\bar{e}'_1 = -\frac{1}{AB}(A^2\bar{e}_1 + \beta\beta_\varphi\bar{e}_2 - \beta_\varphi\bar{e}_3), \tag{20}$$

$$\bar{e}'_2 = \frac{1}{A}(\bar{e}_2 + \beta\bar{e}_3), \tag{21}$$

$$\bar{e}'_3 = \frac{1}{B}(\beta_\varphi\bar{e}_1 - \beta\bar{e}_2 + \bar{e}_3). \tag{22}$$

An important geometric characteristic of ring stents, which affects its mechanical and medical characteristics [33], is the perimeter. By integrating the expression for the arc differential (17) with  $f = x$  and with account of (13), it is possible to determine how the perimeter of the ring (9) changes with the introduction of a pitch function.

Figure 8 reports the effect of the coefficient  $\alpha$  on the change in the perimeter at  $z = \sin nf(\varphi)$ ;  $n = 8$ ;  $h = \frac{H}{R} = 0.3$  for the pitch function (13). With the growth of the parameter  $\alpha$  within the interval of its possible change (14), the perimeter of the corrugated ring slightly increases.

### 5 Equilibrium equations

Let us determine the influence of function (13) on the radial stiffness of a ring with a variable corrugation pitch. To do this, consider its deformation under the action of a uniform external pressure  $q$ . For element of corrugated ring  $AB$  of length  $ds$  and the forces acting on it (Fig. 9), we obtain two vector equilibrium equations

$$\begin{cases} \bar{F}_\varphi + RA\bar{q} = 0, \\ \bar{M}_\varphi + RA\bar{e}'_2 \times \bar{F} = 0. \end{cases} \tag{23}$$

Then, we use the basis expansions

$$\begin{aligned} \bar{F} &= F_1\bar{e}_1 + F_2\bar{e}_2 + F_3\bar{e}_3, \\ \bar{M} &= M_1\bar{e}_1 + M_2\bar{e}_2 + M_3\bar{e}_3, \\ \bar{q} &= q\bar{e}_1, \end{aligned} \tag{24}$$

where  $q = q(\varphi)$ .

Substituting expansions (24) into Eqs. (23), we obtain the following equilibrium equations in projections on the axis of the base circle

$$F_{1\varphi} - F_2 = -RAq, \tag{25}$$

$$F_{2\varphi} + F_1 = 0, \tag{26}$$

$$F_{3\varphi} = 0, \tag{27}$$



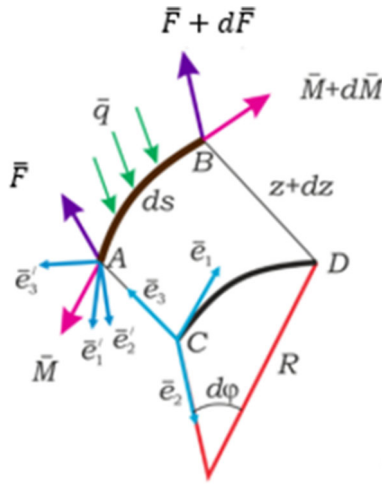


**Fig. 9** The element AB of the corrugated ring (10) ( $\bar{F}$ ,  $\bar{M}$ ,  $\bar{q}$  are the vectors of internal forces, moments and external load;  $CD$  is the projection of the element  $AB$  onto the base circle;  $\bar{e}_1, \bar{e}_2, \bar{e}_3$  are the unit vectors of the tetrahedron associated with the base circle;  $\bar{e}'_1, \bar{e}'_2, \bar{e}'_3$  are the unit vectors of the movable orthogonal coordinate basis associated with the middle line of the corrugated ring:  $\bar{e}'_2$ —tangential,  $\bar{e}'_1$ —along the main normal,  $\bar{e}'_3$ —along the binormal to the middle line;  $\bar{e}'_1 \perp \bar{F}$ )

$$M_{1\varphi} - M_2 + R(F_3 - \beta F_2) = 0, \tag{28}$$

$$M_{2\varphi} + M_1 + R\beta F_1 = 0, \tag{29}$$

$$M_{3\varphi} - RF_1 = 0. \tag{30}$$

Equation (27) and the symmetry condition imply that

$$F_3 = 0. \tag{31}$$

Equations (25), (26) yield

$$F_{2\varphi\varphi} + F_2 = RAq. \tag{32}$$

For  $q = \text{const}$ , using the relations (25), (26), Eq. (30) is reduced to the form

$$M_{3\varphi\varphi\varphi} + M_{3\varphi} = R^2 A\varphi q. \tag{33}$$

Observe that Eq. (33) coincides with the equilibrium equation of a circular ring under the action of variable external pressure [34].

### 6 Homogenization of equilibrium equations

For the calculation and optimal design [35] of regularly corrugated rings, the asymptotic homogenization method (AHM) [36] is employed (for the case of a variable corrugation pitch, the modification of AHM [37] can be used).

Let us introduce a new variable  $\xi = nf(\varphi)$ , which is assumed to be independent on  $\varphi$ . In what follows, the "fast" variable is considered on the interval  $(0, 2\pi)$ . The following differentiations rule holds

$$\frac{d}{d\varphi} = \frac{\partial}{\partial\varphi} + nf_\varphi \frac{\partial}{\partial\xi} \tag{34}$$

The projections of the forces and moments (24) are represented as the series

$$F_i = \sum_{k=0}^{\infty} n^{-k} F_{ik}(\varphi, \xi), \quad M_i = \sum_{k=0}^{\infty} n^{-k} M_{ik}(\varphi, \xi), \tag{35}$$

where  $i = 1 - 3$ ;  $F_{ik}, M_{ik}$  are the  $\xi$ -periodic functions with period  $2\pi$ .

Substituting expansions (34), (35) into Eqs. (25)–(30) and assuming  $f_\varphi\beta \sim 1$ , after splitting in powers of  $n^{-k}$ , one obtains

$$F_{i0\xi} = 0; M_{i0\xi} = 0, \tag{36}$$

$$f_\varphi F_{11\xi} + F_{10\varphi} + F_{20} = RAq, \tag{37}$$

$$f_\varphi F_{21\xi} + F_{20\varphi} + F_{10} = 0, \tag{38}$$

$$f_\varphi M_{11\xi} + M_{10\varphi} - M_{20} - Rf_\varphi\beta F_{20} = 0, \tag{39}$$

$$f_\varphi M_{21\xi} + M_{20\varphi} + M_{10} + Rf_\varphi\beta F_{10} = 0, \tag{40}$$

$$f_\varphi M_{31\xi} + M_{30\varphi} - RF_{10} = 0, \tag{41}$$

where  $\beta = z_\xi$ ;  $A = \sqrt{1 + (nf_\varphi\beta)^2}$ .

Equation (36) yields

$$F_{i0} = F_{i0}(\varphi), \quad M_{i0} = M_{i0}(\varphi). \tag{42}$$

In what follows, we apply to Eqs. (38)–(42) the averaging operator  $\int_0^{2\pi} (\dots)d\xi$ , considering periodicity in  $\xi$  expansions (35), and we get

$$F_{10\varphi} - F_{20} = -Raq, \tag{43}$$

$$F_{20\varphi} + F_{10} = 0, \tag{44}$$

$$M_{10\varphi} - M_{20} = 0, \tag{45}$$

$$M_{20\varphi} + M_{10} = 0, \tag{46}$$

$$M_{30\varphi} - RF_{10} = 0, \tag{47}$$

where  $a(\varphi) = \frac{1}{2\pi} \int_0^{2\pi} Ad\xi$ .

From Eqs. (43)–(46), one obtains

$$F_{20\varphi} + F_{20} = Raq, \tag{48}$$

$$M_{10} = M_{20} \equiv 0. \tag{49}$$

In the future, without loss of generality, we restrict ourselves to a sinusoidal corrugation, and hence,

$$a(\varphi) = \frac{2}{\pi} \sqrt{1 + m^2} E(s), \tag{50}$$

where  $m = nhf_\varphi$ ;  $E(s)$  is the complete elliptic integral of the second kind,  $s^2 = \frac{m^2}{1+m^2}$ .

Expanding  $E(s)$  in powers of  $s$ , we obtain

$$a(\varphi) = 4\sqrt{1 + m^2} \left( 1 - \frac{1}{4} \frac{m^2}{1 + m^2} + O(s^4) \right). \tag{51}$$

For the considered example of function  $f$  (Fig. 6), taking into account the constraint (14), expression (51) can be expanded in powers of  $\alpha \ll 1$ . Restricting ourselves to the first two terms of the expansion, we obtain

$$a(\varphi) = a_0 + \alpha a_1 \left( 5\varphi^4 - 20\pi\varphi^3 + 20\pi\varphi^2 + 40\pi^2(\pi - 1)\varphi + \frac{40}{3}\pi^3 - 16\pi^4 + \frac{1}{\alpha} \right), \tag{52}$$

where

$$a_0 = \sqrt{1 + \hat{h}^2} \left( 1 - \frac{1}{4} \frac{\hat{h}^2}{1 + \hat{h}^2} \right), a_1 = \frac{1}{2} \sqrt{1 + \hat{h}^2} \left( 1 - \frac{1}{2} \frac{\hat{h}^2}{1 + \hat{h}^2} \right) \frac{\hat{h}^2}{(1 + \hat{h}^2)^2}, \hat{h} = nh.$$

To assess the impact on the distribution of force involved in the change in the corrugation pitch, we substitute expression (52) into (48) and write out the general solution of the resulting equation for  $q = \text{const}$

$$F_{20} = C_1 \cos(\varphi) + C_2 \sin(\varphi) + Rq(a_0 + a_1 \left( 1 + \frac{\alpha}{3} (-48\pi^4 + (40 + 120\varphi)\pi^3 - 120\pi^2\varphi + (360\varphi - 60\varphi^3 + 60\varphi^2 - 120)\pi + 360 - 180\varphi^2 + 15\varphi^4) \right)), \quad (53)$$

where  $C_1, C_2$  are integration constants determined from the condition  $q = 0, F_{20} \equiv 0$ .

From here, we have

$$C_1 = C_2 = 0. \quad (54)$$

Using expressions (53), (54), from Eqs. (44), (47), we find that

$$F_{10} = -\alpha Rq a_1 a_2, \quad (55)$$

$$M_{30} = -\alpha R^2 q a_1 a_2, \quad (56)$$

where  $a_2 = 20(6\pi + 2(\pi^2 - 3)\varphi - 3\pi\varphi^2 + \varphi^3)$ .

Thus, for the considered corrugation with a variable pitch (13), the main internal force factor is the force directed tangentially to the circle (53), other force factors are equal to zero or are values of a smaller order of smallness with respect to the value  $\alpha$  (55), (56). It is important to notice that the resulting expressions (53)–(56) satisfy the conjugation conditions of the following form

$$(F_{20}, F_{10}, M_{30})_{\varphi=0} = (F_{20}, F_{10}, M_{30})_{\varphi=2\pi}, \quad (57)$$

and smoothness conditions

$$(F_{20\varphi}, F_{10\varphi}, M_{30\varphi})_{\varphi=0} = -(F_{20\varphi}, F_{10\varphi}, M_{30\varphi})_{\varphi=2\pi}, \quad (58)$$

where  $(\dots)_{\varphi=0, 2\pi}$  mean one-sided derivatives for  $d\varphi^{+, -}$ , respectively.

Conditions for smooth conjugation of expressions for internal force factors (57), (58) are one of the criteria for choosing the function (13).

Figure 10 presents the change of  $F_{20}$  (53) in comparison with the change in the corrugation pitch for function (13) at  $\hat{h} = 0.8; \alpha = 0.0005$ ; line 2—development of the corrugated ring.

Thus, with a decrease (increase) in the corrugation pitch, the value of  $F_{20}$  increases (decreases).

## 7 Displacement and strain equations

The deformation of the axial line of the corrugated ring is considered in a linear formulation. Let, as a result of deformation, the points of the axial line receive small displacements  $U_i(\varphi) \ll R$  in the basis associated with the circle (Fig. 5). Then, the radius vector of the axial line after deformation can be written as

$$\tilde{r} = R((1 + u_1)\bar{e}_1(\varphi + u_2) + (z(\varphi + u_2) + u_3)\bar{e}_3(\varphi + u_2)), \quad (59)$$

where  $u_i = \frac{U_i}{R} \ll 1$ .

Expanding the functions in (59) in powers of  $\varphi$  and leaving only the linear terms, we obtain

$$\tilde{r} = R((1 + u_1)\bar{e}_1 + u_2\bar{e}_2 + (z + \beta u_2 + u_3)\bar{e}_3). \quad (60)$$

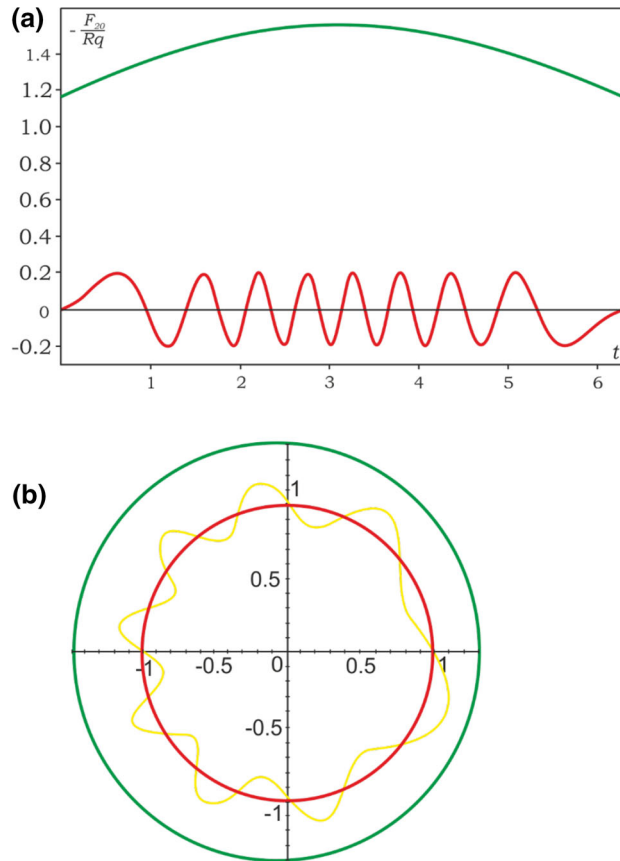


**Fig. 10 a** Magnitude dependency  $-\frac{F_{20}}{Rq}$  (53) (green curve) from the change in the corrugation pitch for the function (13) of the sinusoidal corrugation at  $n = 8$ ;  $\hat{h} = 0.8$ ;  $\alpha = 0.0005$ ; red curve—corrugated ring development. **b** Dependency diagram  $-\frac{F_{20}}{Rq}$  yielded by formulas (53) (green curve) with an account of the change in the corrugation pitch in the polar co-ordinates

Substituting the expression for the radius vector (60) into formula (17) and restricting ourselves to linear terms, we find

$$d\tilde{s} = |\tilde{r}_\varphi| d\varphi = RA \sqrt{1 + \frac{2}{A^2} (u_1 + u_{2\varphi} + \beta(u_{3\varphi} + \beta_\varphi u_2 + \beta u_{2\varphi}))} d\varphi. \quad (61)$$

Let us assume that the linear deformation of the ring under the action of a distributed load  $q$  (Fig. 5) occurs only due to bending, then  $d\tilde{s} = ds$  and

$$u_1 + u_{2\varphi} + \beta(u_{3\varphi} + \beta_\varphi u_2 + \beta u_{2\varphi}) = 0. \quad (62)$$

Let us assume that the basic round ring (Fig. 4) is inextensible with regard to the axial line, and find the relationship between its radial deformation

$$\epsilon = \frac{2\pi R - 2\pi(R - u_1)}{2\pi R} = \frac{u_1}{R} \quad (63)$$

and the value of external pressure  $q$ . Since the force  $F_{20}$  (53) is the main force factor for the considered external load, to assess the effect of a variable corrugation pitch on the radial stiffness of the ring, we restrict ourselves to the analysis of deformation (63).

The main step in AHM is to solve the problem on the cell, i.e., problem on a periodically repeating element. With a sufficiently large number of corrugation waves, the curvature of the ring can be neglected in the cell problem.

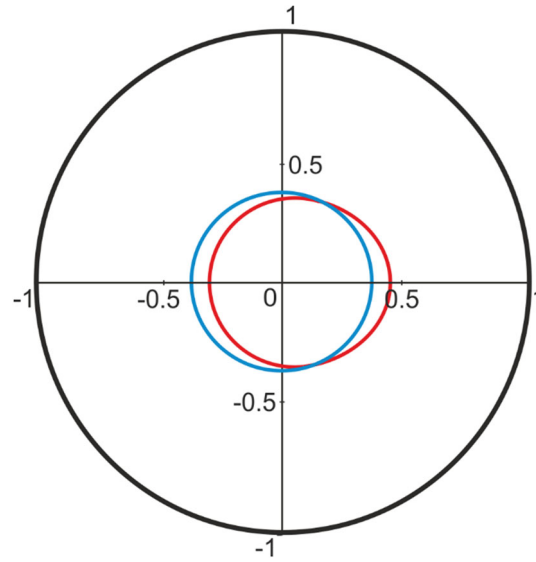


**Fig. 11** Radial deformation (67)  $\frac{ku_1}{\frac{h^2 R^2 q}{EI}}$  (red line); blue line—regular corrugation deformation ( $\alpha = 0$ ) the same perimeter; black line – base circle ( $R = 1, n = 8, \hat{h} = 0.8, \alpha = 0.0004, k = 0.5$ ).. (Color figure online)

As a result, taking into account the condition of non-extensibility of the axial line (62), we get the dependence between the force  $F_{20}$  and the deformation of the base circle

$$F_{20} = \epsilon^{-1} u_{20\varphi}, \tag{64}$$

where

$$\epsilon = \frac{h^2}{EI} \frac{1}{2\pi} \int_0^{2\pi} z^2 A d\xi, \tag{65}$$

and  $E$  is the elastic modulus of the material, while  $I$  is the moment of inertia of the transverse cross section of the stent fibers. Equating the tangential (63) and axial (64) deformations, we obtain the dependence of the radial displacement  $u_1$  on the corrugation pitch at a uniform external pressure

$$u_1 = \epsilon R F_{20}. \tag{66}$$

For the considered function (13), expanding expression (65) in powers  $\alpha$  and substituting the expression (53), (54) into (66), restricting ourselves to terms of zero and first degree  $\alpha$ , we get ( $n = 8; \hat{h} = 0.8$ )

$$u_1 = \frac{h^2 R^2 q}{EI} (0.62 + \alpha(0.94\varphi^4 - 11.84\varphi^3 + 5.36\varphi^2 + 200.08\varphi - 216.47)). \tag{67}$$

Figure 11 reports the radial deformation (67) at  $\alpha = 0.0004$  and for  $\alpha = 0$  (deformation of the ring with a constant corrugation pitch of the same length of the axial line). Note that, for  $\alpha = 0$ , deformation (66) coincides with the expression obtained in [34].

It follows from Fig. 12 that a decrease in the corrugation pitch reduces the radial rigidity of the corrugated ring. At the same time, this decrease is significantly affected by the value of the coefficient  $\alpha$ . It follows from expression (67) that for the considered function (13), the greatest (least) radial stiffness  $g(\varphi)$  has a corrugated ring with a variable pitch at

$$g_{max} = g(0), \tag{68}$$

$$g_{min} = g(\pi). \tag{69}$$

It should be emphasized that the conditions (68), (69) are important in the orientation of the stent in relation to the vascular plaque.

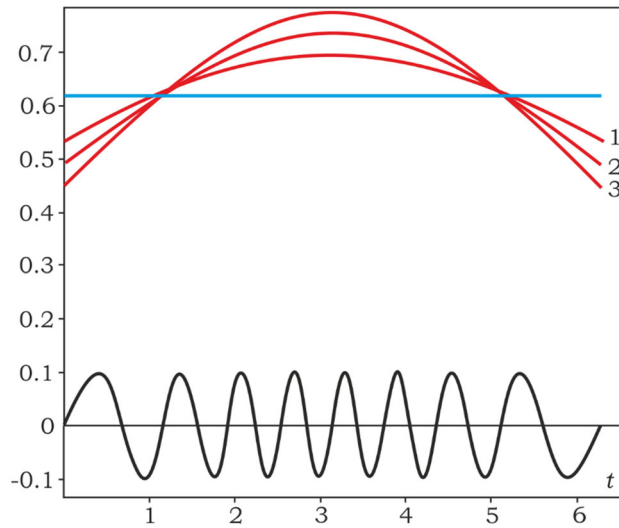


**Fig. 12** Deformation  $\frac{ku_1}{h^2 R^2 q}$  at different values of the coefficient  $\alpha$ : 1 – 0.0005; 2 – 0.0006; 3 – 0.0008.

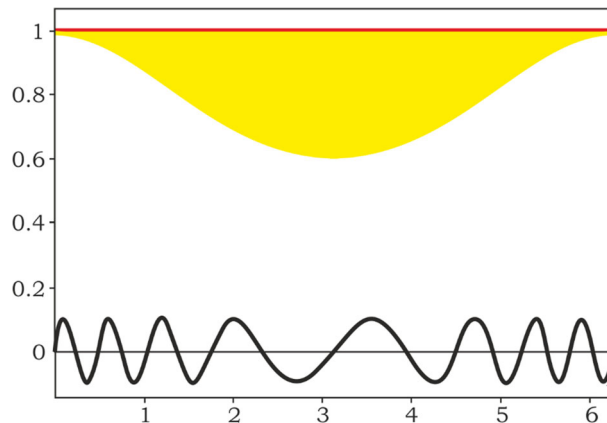


**Fig. 13** Developments of plaque (5) and stent corrugation (70) for  $a = 0.003, e = 0.01, h = 0.1, \alpha = 0.0025$

**8 Evaluation of the effectiveness of the use of variable pitch corrugations**

Consider the radial deformation of a corrugated ring with a variable pitch (13) under the action of an external load (8). Let us match the points of maximum radial stiffness of the corrugated ring (68) and the maximum intensity of the load (7). To do this, turn the corrugated ring (Fig. 6a) through an angle equal to  $\pi$ . New function  $\hat{f}$ , in this case, can be found by expanding the expression  $\frac{1}{f_\varphi}$  in powers of  $\alpha$ , restricting ourselves to terms no higher than the first degree, and integrating the resulting expression

$$\hat{f} = \varphi - \alpha \left( \varphi^5 - 5\pi\varphi^4 + \frac{20}{3}\varphi^3 - \frac{8}{3}\pi^4\varphi \right). \tag{70}$$

The development of the plaque (5) and the corresponding corrugation of the stent (70) are shown in Fig. 13. To assess the effectiveness of the use of a variable pitch corrugation, we restrict ourselves to radial deformation caused by the main internal force factor  $F_{20}$ . Substituting expressions for external load (7) and function (70) into Eq. (48), after integration and using expression (66), we obtain an expression for  $u_{1c}$ , which is not shown due to its cumbersome nature. Figure 14 shows a comparison of deformation  $u_{1c}$  and  $u_1$ , i.e., deformation of a regularly corrugated ring of the same perimeter, for the following fixed parameters:  $R = 1, a = 0.003, d = 0.01, n = 8, \hat{h} = 0.8, \alpha = 0.0008, k = 0.5$ .

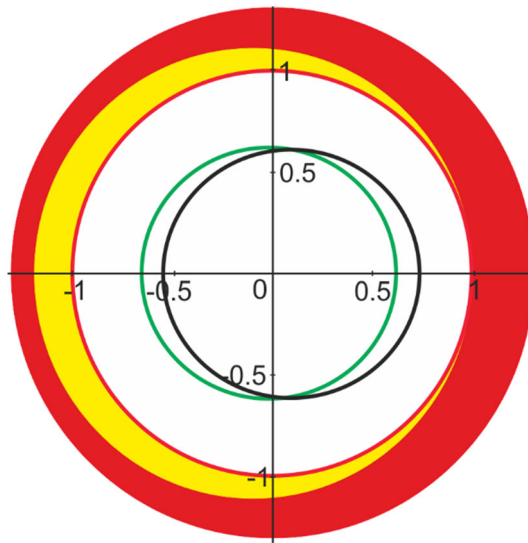


**Fig. 14** Comparison of radial deformation of the ring with variable pitch corrugation (green line) and with a regularly corrugated ring of the same perimeter (black line) for  $R = 1, a = 0.003, d = 0.01, n = 8, \hat{h} = 0.8, \alpha = 0.0008, k = 0.5, \hat{u}_1 = \frac{k u_1}{h^2 R^2 q}, \hat{u}_{1c} = \frac{k u_1}{E I}$ .

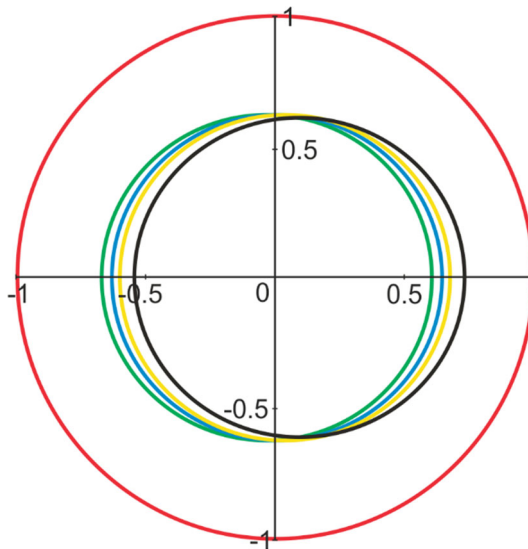


**Fig. 15** Dependence of the deformation of a corrugated ring with a variable pitch (Fig. 14) with respect to the value of the coefficient  $\alpha$ : 0.0008 (green line); 0.0006 (blue line); 0.0004 (yellow line); 0 (black line); red line—inner wall of the vessel after ballooning. (Color figure online)

Thus (Fig. 14), the use of a corrugation with a variable pitch (70) reduces the deformation in the more loaded part of the ring, but increases it in the less loaded one. The latter fact reduces the efficiency of variable pitch corrugation.

Figure 15 presents the dependence of the deformation of a corrugated ring with a variable pitch of corrugations (Fig. 14) versus the value of the coefficient  $\alpha$ .

The case study of vascular stents is to provide a lumen for the flow of blood after ballooning. Therefore, the effectiveness of the stent can be assessed by the area of this lumen after deformation. Let us compare the areas bounded by the deformation lines of a corrugated ring with a variable pitch  $S_c$  and regularly corrugated  $S$ . Figure 16 shows the dependence of the relative increase in lumen, which provides a corrugated ring with a

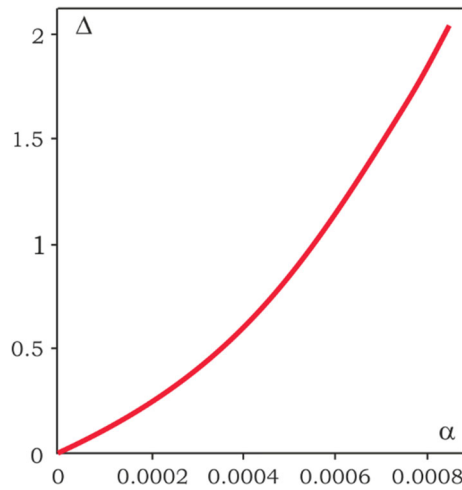


**Fig. 16** The dependence of the relative increase in the lumen, which provides a corrugated ring with a variable pitch in relation to a regularly corrugated ring ( $\Delta = \frac{S_c - S}{S} 100\%$ ) on the value of the coefficient  $\alpha$  (70)

variable pitch in relation to a regularly corrugated ring ( $\Delta = \frac{S_c - S}{S} 100\%$ ) on the value of the pitch factor  $\alpha$  (70).

Thus, a stent with variable pitch corrugated rings is more effective than a stent with regularly corrugated ones.

## 9 Concluding remarks

A possible design of a patient-specific vascular stent is analyzed, taking into account the geometry of vascular plaques. An integral element of many types of stents is a corrugated ring. It is proposed to replace the corrugation with a constant pitch to corrugations with variable pitch. The goal is widening of the lumen of blood vessels. The function that describes the variability of corrugations pitch is derived. It is shown that the proposed modification of corrugation can be more effective than the known standard design of vascular stent ring.

However, it should be mentioned that the plaque is modeled as idealized, and it suffers for introduction of various simplifications in terms of geometry and material. Clinical evidence of the anatomical features should be provided to correctly address such modeling choices. With regard to the stent, several nonlinearities should be future considered to model the stent insertion into the catheter and the implantation into the vessel, such as the material (plasticity for balloon-expandable or super-elasticity for self-expandable stents). Also, a variable corrugated pitch could lead to structural instabilities during the stent crimping and, consequently, to the failure throughout the insertion in the catheter. The problem of correctly positioning the stent in the circumferential direction during the implantation procedure should be discussed in future as well.

**Author contributions** IA and JA wrote the main manuscript text; JA prepared Figs. 3, 5, 6, 7, 8, 9, 10, 11, 12, 13, 14, 15 and 16. All authors reviewed the manuscript.

**Funding** No funding has supported this research.

## Declarations

**Conflict of interest** The authors declare that there is no conflict of interest regarding the publication of this article.

**Open Access** This article is licensed under a Creative Commons Attribution 4.0 International License, which permits use, sharing, adaptation, distribution and reproduction in any medium or format, as long as you give appropriate credit to the original author(s) and the source, provide a link to the Creative Commons licence, and indicate if changes were made. The images or other third party material in this article are included in the article's Creative Commons licence, unless indicated otherwise in a credit line to the material. If material is not included in the article's Creative Commons licence and your intended use is not permitted



by statutory regulation or exceeds the permitted use, you will need to obtain permission directly from the copyright holder. To view a copy of this licence, visit <http://creativecommons.org/licenses/by/4.0/>.

## References

- Colombo, A., Stankovic, G., Moses, J.W.: Selection of coronary stents. *J. Am. Coll. Cardiol.* **40**, 1021–1033 (2002)
- Grewe, P.H., Deneke, T., Machraoui, A., Barmeyer, J., Muller, K.M.: Acute and chronic tissue response to coronary stent implantation: pathologic findings in human specimens. *J. Am. Coll. Cardiol.* **35**, 157–163 (2000)
- Tan, L.B., Webb, D.C., Kormi, K., Al-Hassani, S.T.S.: A method for investigating the mechanical properties of intracoronary stents using finite element numerical simulation. *Int. J. Cardiol.* **78**, 51–67 (2001)
- Petrini, L., Migliavacca, F., Auricchio, F., Dubini, G.: Numerical investigation of the intravascular coronary stent flexibility. *J. Biomech.* **37**, 495–501 (2004)
- Edelman, E.R., Rogers, C.: Pathobiologic responses to stenting. *Am. J. Cardiol.* **81**, 4E–6E (1998)
- Hoffman, R., Mintz, G.S., Mehran, R., Kent, K.M., Pichard, A.D., Satler, L.F., Leon, M.B.: Tissue proliferation within and surrounding Palmaz-Schatz stents is dependent on the aggressiveness of the stent implantation technique. *Am. J. Cardiol.* **83**, 1170–1174 (1999)
- Kastrati, A., Dirschinger, J., Boekstegers, P., Elezi, S., Schuchlen, H., Pache, J., Steinbeck, G., Schmitt, C., Ulm, K., Neumann, F.J., Schomig, A.: Influence of stent design on 1-year outcome after coronary stent placement: a randomized comparison of five stent types in 1,147 unselected patients. *Catheteriz. Cardiovasc. Interv.* **50**, 290–297 (2000)
- Rogers, C., Tseng, D.Y., Squire, J.C., Edelman, E.R.: Balloon–artery interactions during stent placement. A finite element analysis approach to pressure, compliance, and stent design as contributors to vascular injury. *Circ. Res.* **84**, 378–383 (1999)
- Auricchio, F., Di Loreto, M., Sacco, E.: Finite-element analysis of a stenotic artery revascularization through a stent insertion. *Comput. Methods Biomech. Biomed. Eng.* **4**, 249–326 (2001)
- Holzappel, G.A., Stadler, M., Schulze-Bauer, C.A.J.: A layer-specific three-dimensional model for the simulation of balloon angioplasty using magnetic resonance imaging and mechanical testing. *Ann. Biomed. Eng.* **30**, 753–767 (2002)
- Lally, C., Dolan, F., Prendergast, P.J.: Cardiovascular stent design and vessel stresses: a finite element analysis. *J. Biomech.* **38**, 1574–1581 (2005)
- Timmins, L.H., Meyer, C.A., Moreno, M.R., Moore, J.E.: Effects of stent design and atherosclerotic plaque composition on arterial wall biomechanics. *J. Endovasc. Ther.* **15**, 643–654 (2008)
- Timmins, L.H., Miller, M.W., Clubb-Jr, F.J., Moore-Jr, J.E.: Increased artery wall stress post-stenting leads to greater intimal thickening. *Lab. Investig.* **91**, 955–967 (2011)
- Schmidt, W., Wissgott, Ch., Brandt-Wunderlich, Ch., Behrens, P., Schmitz, K.P., Grabow, N., Andresen, R.: Biomechanics and clinical experience of a 3D biomimicking vascular stent. *Curr. Dir. Biomed. Eng.* **4**(1), 135–139 (2018)
- Kokot, G., Kuś, W., Dobrzyński, P., Sobota, M., Smola, A., Kasperczyk, J.: A project of bioresorbable self-expanding vascular stents. The crimping process numerical simulation. *AIP Conf. Proc.* **1922**, 07000 (2018)
- Qiu, T.Y., Song, M., Zhao, L.G.: A computational study of crimping and expansion of bioresorbable polymeric stents. *Mech. Time-Depend. Mater.* **22**, 273–290 (2018)
- Wei, Y., Wang, M., Zhao, D., Li, H., Jin, Y.: Structural design of mechanical property for biodegradable polymeric stent. *Adv. Mater. Sci. Eng.* **2019**, 2960435 (2019)
- Liu, P., Deng, X., Liu, X., Sun, A., Kang, H.: Influence of artery straightening on local hemodynamics in left anterior descending (LAD) artery after stent implantation. *Cardiol. Res. Pract.* **2020**, 6970817 (2020)
- Bernini, M., Colombo, M., Dunlop, C., Hellmuth, R., Chiastra, C., Ronan, W., Vaughan, T.J.: Oversizing of self-expanding Nitinol vascular stents—a biomechanical investigation in the superficial femoral artery. *J. Mech. Behav. Biomed. Mater.* **132**, 105259 (2022)
- Auricchio, F., Conti, M., Beule, M.D., Santis, G.D., Verheggh, B.: Carotid artery stenting simulation: from patient-specific images to finite element analysis. *Med. Eng. Phys.* **33**, 281–289 (2011)
- Morlacchi, S., Colleoni, S.G., Cárdenes, R., Chiastra, C., Diez, J.L., Larrabide, I., Migliavacca, F.: Patient-specific simulations of stenting procedures in coronary bifurcations: two clinical cases. *Med. Eng. Phys.* **35**, 1272–1281 (2013)
- Ragkousis, G.E., Curzen, N., Bressloff, N.W.: Simulation of longitudinal stent deformation in a patient-specific coronary artery. *Med. Eng. Phys.* **36**, 467–476 (2014)
- Han, Y.F., Lu, W.F.: Optimizing the deformation behavior of stent with non-uniform Poisson’s ratio distribution for curved artery. *J. Mech. Behav. Biomed.* **88**, 442–452 (2018)
- Pan, Ch., Han, Y., Lu, J.: Structural design of vascular stents: a review. *Micromachines* **12**, 770–777 (2021)
- He, R., Zhao, L., Silberschmidt, V.V., Feng, J., Serracino-Inglott, F.: Personalised nitinol stent for focal plaques: design and evaluation. *J. Biomech.* **130**, 110873 (2022)
- Awrejcewicz, J.: *Classical Mechanics. Kinematics and Statics.* Springer, Berlin (2012)
- Awrejcewicz, J.: *Classical Mechanics. Dynamics.* Springer, Berlin (2012)
- Andrianov, I.V., Awrejcewicz, J., Diskovsky, A.A.: Optimal design of a functionally graded corrugated rods subjected to longitudinal deformation. *Arch. Appl. Mech.* **85**(2), 303–314 (2015)
- Andrianov, I.V., Diskovsky, A.A., Syerko, E.: Optimal design of a circular corrugated diaphragm using the homogenization approach. *Math. Mech. Solids* **22**(3), 283–303 (2017)
- Andrianov, I.I., Awrejcewicz, J., Diskovsky, A.A.: Optimal design of a functionally graded corrugated cylindrical shell subjected to axisymmetric loading. *Arch. Appl. Mech.* **88**(6), 1027–1039 (2018)
- Andrianov, I.I., Awrejcewicz, J., Diskovsky, A.A.: The optimal design of a functionally graded corrugated cylindrical shell under axisymmetric loading. *Int. J. Nonlinear Sci. Numer. Simul.* **20**(3–4), 387–398 (2019)
- Tap, K.: *Differential Geometry of Curves and Surfaces.* Springer, New York (2016)
- Borhani, S., Hassanajili, S., Ahmadi Tafti, S.H., Rabbani, S.: Cardiovascular stents: overview, evolution, and next generation. *Prog. Biomater.* **7**(3), 175–205 (2018)

- 
34. Timoshenko, S., Gere, J.: *Theory of Elastic Stability*. McGraw-Hill, New York (1961)
  35. Andrianov, I.V., Awrejcewicz, J., Diskovsky, A.A.: Optimal design of the vascular stent ring in order to maximise radial stiffness. *Arch. Appl. Mech.* **92**, 667–678 (2022)
  36. Andrianov, I.V., Awrejcewicz, J., Manevitch, L.I.: *Asymptotical Mechanics of Thin-Walled Structures: A Handbook*. Springer, Berlin (2004)
  37. Andrianov, I.V., Awrejcewicz, J., Diskovsky, A.A.: Homogenization of quasi-periodic structures. *J. Vib. Acoust.* **128**(4), 532–534 (2006)

**Publisher's Note** Springer Nature remains neutral with regard to jurisdictional claims in published maps and institutional affiliations.